From glucose to enantiopure morpholino β-amino acid: a new tool

From glucose to enantiopure morpholino β-amino acid: a new tool for stabilizing γ-turns in peptides

Raffaella Bucci, Alessandro Contini,* Francesca Clerici, Sara Pellegrino, Maria Luisa Gelmi*

DISFARM-Sez. Chimica Generale e Organica "A. Marchesini", Università degli Studi di Milano, via Venezian 21, 20133 Milano, Italy

Corresponding author: E-mail: marialuisa.gelmi@unimi.it

A new cyclic enantiopure β-amino acid, named β-Morph, containing the morpholino ring, was obtained in gram scale starting from α-D-glucopyranose enantiopure material, focusing on the "environmental sustainability" concept. A series of ultrashort model peptides containing β-Morph were prepared. β-Morph was found able to induce an inverse γ-turn in Leu-Val containing sequences. Key element for the γ-turn formation might be the oxygen atom of morpholino ring that could drive the spatial orientation of NH of amino acid *i*+1, through an unusual hydrogen bond. This datum was confirmed by QTAIM calculations. Interestingly, when two β-Morph-Leu-Val repeats are present in the peptide, two γ-turns can be formed, as supported by NMR experiments and aMD and H-REMD calculations.

Introduction

γ-Turns is a very short motif able to reverse the main chain of a peptide/protein. It is stabilized by the formation of a hydrogen bond between the C=O of residue *i* and the NH of residue *i*+2 forming a pseudo-seven-membered ring. Depending on the ϕ and ψ angles, two different type of turns can be designed defined as inverse [φ (-75°); ψ (+65°)] and classical φ (+75°); ψ (-65°)] γ-turns. In the first one, the R substituent of the α-amino acid lies in the equatorial position, while in the second one in axial position. Inverse γ-turns are generally located at a position of reversal in chain direction (180°) and often within β-strands associated to β-sheets. On the other hand, classical γ-turns are less common in proteins, and in most cases, they lie at the loop end of a β-hairpin.[1]

for stabilizing γ-turns in peptides

Raffaella Bucci, Alessandro Contini,* Francesca Clerici, Sara Pellegrino, Maria Luisa Gelmi*

DISFARM-Sez. Chimica Generale e Organica "A. Marchesini", Università degli Studi di Milano, via Venezian 21, 20133 Milano, Italy

Corresponding author: E-mail: marialuisa.gelmi@unimi.it

A new cyclic enantiopure β-amino acid, named β-Morph, containing the morpholino ring, was obtained in gram scale starting from α-D-glucopyranose enantiopure material, focusing on the "environmental sustainability" concept. A series of ultrashort model peptides containing β-Morph were prepared. β-Morph was found able to induce an inverse γ-turn in Leu-Val containing sequences. Key element for the γ-turn formation might be the oxygen atom of morpholino ring that could drive the spatial orientation of NH of amino acid *i*+1, through an unusual hydrogen bond. This datum was confirmed by QTAIM calculations. Interestingly, when two β-Morph-Leu-Val repeats are present in the peptide, two γ-turns can be formed, as supported by NMR experiments and aMD and H-REMD calculations.

Introduction

γ-Turns is a very short motif able to reverse the main chain of a peptide/protein. It is stabilized by the formation of a hydrogen bond between the C=O of residue *i* and the NH of residue *i*+2 forming a pseudo-seven-membered ring. Depending on the ϕ and ψ angles, two different type of turns can be designed defined as inverse [φ (-75°); ψ (+65°)] and classical φ (+75°); ψ (-65°)] γ-turns. In the first one, the R substituent of the α-amino acid lies in the equatorial position, while in the second one in axial position. Inverse γ-turns are generally located at a position of reversal in chain direction (180°) and often within β-strands associated to β-sheets. On the other hand, classical γ-turns are less common in proteins, and in most cases, they lie at the loop end of a β-hairpin.[1]

Even if less abundant of β-turns, γ-turns populate several proteins,[2] such as globular proteins,[3] neurohypophysial peptide hormone vasopressin and derivatives,[4] Mucin protein (MUC1),[5] containing consecutive inverse γ-turns giving rise a S-shape backbone, and hormone angiotensin II.[6]

A selection of natural amino acids able to induce this motif in proteins is well documented.[2] Recently, an overview focused on this motif in peptides/cyclic peptides has been reported by Crisma *et al.*.[7] The importance of non-natural amino acids able to induce this motif emerged from the recent literature.[8–11]

In our research group, we actively work on the development of new non-coded amino acids.[12–15] Some of them were recently used to prepare peptides characterized by defined secondary conformations as well as by different interesting applications.[16–21]

Here, we report on the preparation of a new cyclic enantiopure β-amino acid, *i.e.* the morpholino β-amino acid named β-Morph **1** (Figure 1). Focusing on the "environmental sustainability" concept, compound **1** was prepared in few steps and in gram scale, avoiding isolation and purification of some intermediates, from inexpensive α-D-glucopyranose (**2**) as enantiopure starting material. The features of this amino acid make it very attractive and an interesting tool. Moreover, the presence of an oxygen atom at position 1 of the ring, acting as a H-bond acceptor, could stabilize and/or induce specific secondary structures in peptides.

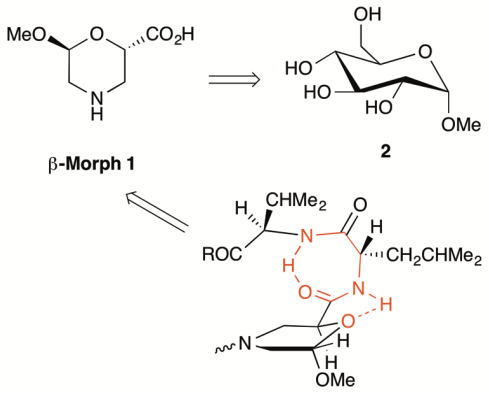

Figure 1. Retrosynthetic scheme to obtain β-morpholino containing peptides.

β-Morph **1** is an analogous of nipecotic acid, deeply studied by Gellman[22] as an effective β-turn inducer. To the best of our knowledge, only two examples of peptide containing the oxazino- or benzoxazino-2-carboxylic acid ring are reported in literature but without peptide conformational studies.[23,24] Focusing on the oxygen morpholino region, several new peptidomimetics containing regiosomeric sugar amino acids building blocks, named SAAs, were prepared.[25–29] Among them, the peptide containing SSAIα, presenting some similarity to β-Morph **1**, showed an extended

conformation.[29] According to this literature overview, it seems that neither the oxygen of the ring nor the acetal function can direct the conformation of the peptide.

It is known that the intrinsic property of natural and non-natural amino acids in generating a specific conformation is also affected and/or reinforced by its environment, *i.e.* by the properties of its nearest and second-nearest neighbours.[30] To evaluate the ability of compound **1** to induce a specific conformation, in this work, we prepared peptide models containing the Leu-Val dipeptide, which is prone to give an extended conformation. Unexpectedly, both NMR and computational studies demonstrated that amino acid **1** acts as a γ-turn inducer. We envisaged in the presence of morpholino oxygen atom the responsibility of drawing the formation of this motif.

Results

*Synthesis of (+)-β-Morph **5***. The new amino acid (+)-**5** was synthesized in enantiopure form starting from the inexpensive and commercially available α-D-glucopyranose (**2**) (Scheme 1).

The first two synthetic steps to obtain the morpholino derivative **3** are reported in the literature,[31] consisting in an oxidative step followed by a reductive amination. In order to avoid the formation of 2*R*-hydroxy-3-[(1-hydroxy-3-oxopropan-2-yl)oxy]-3*S*-methoxypropanal by-product, the oxidation was performed using a large amount of $NaIO_4$ (5 equiv., MeOH/H_2O, 0 °C, 16 h). After work-up, di-aldehyde **A** was formed and directly used for the reductive amination reaction. Applying the synthetic protocol reported in the literature, *i.e.* by adding $NaBH_3CN$ (5 equiv.) to a mixture of aldehyde **A** (3 equiv.) and benzylamine (1 eq., MeOH, 25 °C, 24 h, pH 7), the desired product **3** was isolated in only 50% yield. The reported protocol was modified decreasing the amount of aldehyde **A** (1 eqiv.; MeOH, 25 °C). $NaBH_3CN$ (5 equiv.) and benzylamine (1 equiv.) were added and AcOH was dropped until pH 7. A further batch of benzylamine (2 equiv.) was added after 12 h, affording product (+)-**3** (16 h) in good overall yield (78%) from **2**.

Compound (+)-**3** was then deprotected at nitrogen atom, but the isolation of the free amine was difficult. A one-pot nitrogen deprotection/Boc-protection reaction of amine intermediate (+)-**3** was developed [H_2 (1 atm), Pd/C (10% loading), THF, Boc_2O (1.2 eq.), 25 °C, 2 h] affording compound (+)-**4** in good yields (87 %).

The oxidation of the alcohol function, giving the final *N*-Boc-β-amino acid (+)-**5**, was then studied. Different oxidants were tested. Both 2,2,6,6-tetramethylpiperidine-1-oxyl radical (TEMPO)[0.1 equiv. in the presence of (diacetoxyiodo)benzene (BIAB, 2.2 equiv.), MeCN] and $KMnO_4$ [5 equiv., in the presence of $CuSO_4 \cdot 5H_2O$ (2 equiv.), MeCN] failed giving **5** in low yield. Starting from (+)-**4** (4 equiv.), a successful protocol was achieved consisting in a phase-transfer oxidation

procedure [TEMPO (1 equiv.), NaClO (0.02 equiv.), TBABr (0.3 eqiv.), KBr (0.4 eqiv.),] operating in 1M solution of $NaHCO_3$ and CH_2Cl_2 at 25 °C.[32] After 2h, β-Morph (+)-**5** was obtained in very good yield (83%).

Finally, starting from the α-D-glucopiranoside (**2**), the optimized synthetic protocol was scaled-up (5 g) and the enantiopure new β-Morph-AA (+)-**5** was obtained in 56 % overall yield.

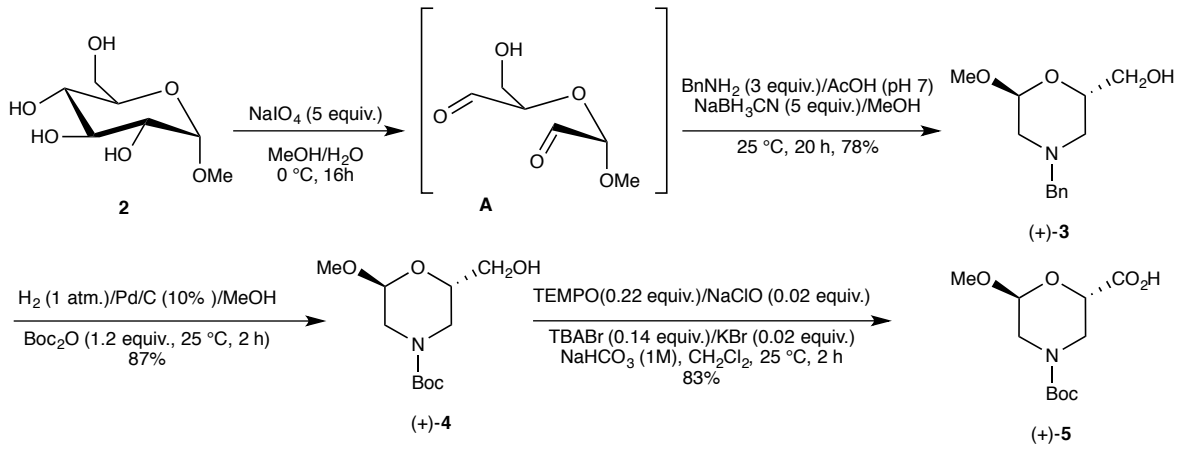

Scheme 1. Synthesis of compound **5**

Peptide synthesis. To evaluate the role of β-Morph-AA **1** in peptide folding, model peptides containing Leu-Val sequence were prepared. This dipeptide was selected due to its intrinsic propensities in giving extended conformations. Considering the importance of the *C*-terminus in stabilizing the secondary structure of a peptide, both the amido-tripeptide **7a** and the corresponding ester **7b** were prepared. Finally, longer pentapeptide **10** and hexapeptide **12**, containing two β-morpholino moieties, were also synthesized. (Table 1)

Table 1. Synthesized peptides

Compd.	**Peptide**	**PM** $[M+Na]^+$
(+)-**7a**	*N*-Boc-(+)-β-Morph-*L*-Leu-*L*-Val-NH_2	496.58
(+)-**7b**	*N*-Boc-(+)-β-Morph-*L*-Leu-*L*-Val-OBn	586.56
(+)-**10**	*N*-Boc-*L*-Val-Gly-(+)-β-Morph-*L*-Leu-*L*-Val-NH_2	651.3
(+)-**12**	*N*-Boc-(+)-β-Morph-*L*-Leu-*L*-Val-(+)-β-Morph-*L*-Leu-*L*-Val-OBn	942.60

The above peptides were prepared by solution phase peptide synthesis using standard protocols (Scheme 2). The condensation reaction was performed by activation of the carboxylic acid (1

equiv.) with HOBT (1.1 equiv.) and EDC (1.1 equiv.) in CH_2Cl_2 (0 °C, 1 h). Free amine (1 equiv.) was then dissolved in CH_2Cl_2 and added to the reaction mixture together with DIEA (2 equiv.; overnight stirring at 25 °C). The *N*-deprotection step was achieved in a solution of TFA/CH_2Cl_2 (1:1; 2h, 25 °C).

By applying these conditions, compound (+)-**5** was coupled with dipeptide NH_2-*L*-Leu-*L*-Val-NH_2 (**6a**) affording tripeptide *N*-Boc-(+)-β-Morph-*L*-Leu-*L*-Val-NH_2 [(+)-**7a**; 95 %], and with NH_2-*L*-Leu-*L*-Val-OBn (**6b**) leading to tripeptide *N*-Boc-(+)-β-Morph-*L*-Leu-*L*-Val-OBn [(+)-**7b**; 69%].

Pentapeptide *N*-Boc-*L*-Val-Gly-(+)-β-Morph-*L*-Leu-*L*-Val-NH_2 (+)-**10** was obtained after Boc-deprotection of **7a**, affording **8a** (97%), and condensation with *N*-Boc-*L*-Val-GlyOH (**9**, 89%). The synthesis is very efficient and pentapeptide (+)-**10** was obtained from **5** with an excellent overall yield (82%) (Scheme 2).

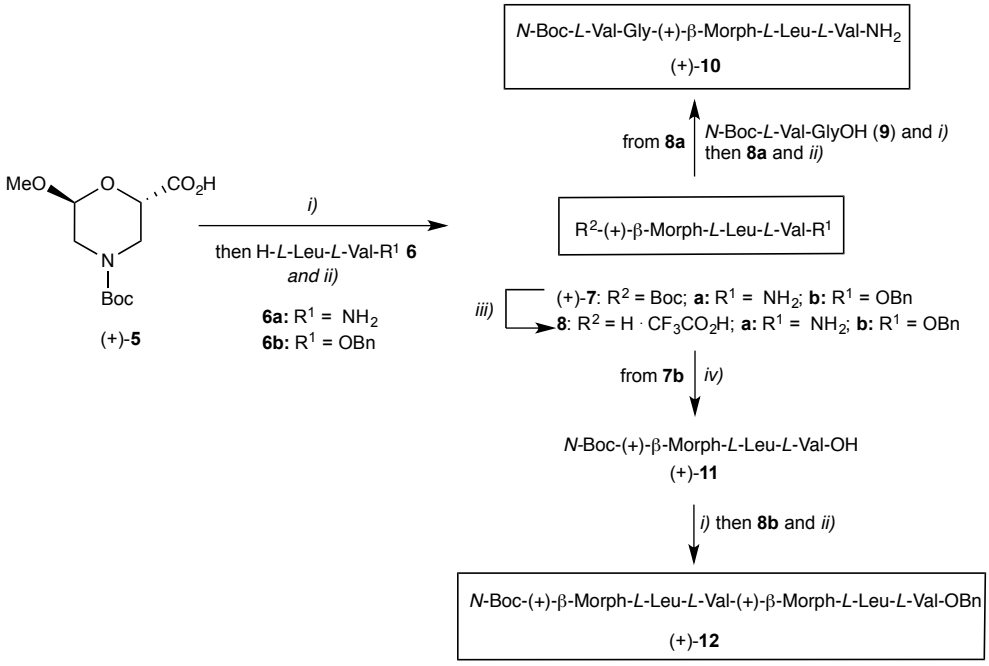

Scheme 2. *i)* HOBT (1.1 equiv.)/EDC (1.1 equiv.)/CH_2Cl_2 (0 °C, 1 h); *ii)* DIEA (2 equiv.)/CH_2Cl_2 (overnight, 25 °C); *iii)* TFA/DCM (1:1; 2h, 25 °C); *iv)* H_2, Pd/C (10%), THF, 1 atm, 25 °C, 2 h.

In a similar way, hexapeptide *N*-Boc-(+)-β-Morph-*L*-Leu-*L*-Val-(+)-β-Morph-*L*-Leu-*L*-Val-OBn [(+)-**12**, 50%] was obtained through Boc deprotection of compound (+)-**7b** (95%) and coupling with *N*-Boc-(+)-β-Morph-*L*-Leu-*L*-Val-OH (+)-**11**. This last compound was obtained by carboxylic function of (+)-**7b** deprotection under H_2 atmosphere (10% Pd/C, THF, 25 °C, 2 h, 93%). The condensation of (+)-**11** with (-)-**8b** gave (+)-**12** in 50 % yield.

All peptides were purified by flash silica gel column chromatography and fully characterized by NMR and ESI-MS.

NMR studies of peptides ***7a,b, 10*** *and* ***12.***

All peptides were characterized in solution by NMR (^{1}H, ^{13}C, COSY, TOCSY, HMBC, HMQC, NOESY; MeCN-d_3, 500 MHz) that allowed assigning unequivocally the chemical shift of each morpholino ring proton as well as of the α-amino acid moieties (Tables S1-S6, ESI). As general features of all studied peptides, well dispersed amide protons are present in the 7-6 ppm region. Furthermore, negative $\Delta\delta_{H\alpha}$ and $\Delta\delta_{NH}$ chemical shifts with respect to random coil structures were detected. $J_{NH/H\alpha}$, values are larger than 8 Hz for both amino acids and are consistent with computational data (see below). All these features suggest that the β-Morph-Leu-Val sequence can assume ordered conformations.

Protons chemical shifts and NOEs of morpholino ring of **7a**, characterized by *S,S*-absolute configuration at C-2 and C-6 (Figure 2A), are shown in Figure 2B. Of relevance, the Noesy experiment (Figure S2, ESI) showed spatial proximity between H-2 and Boc (w) and between this last and H-5 (δ 3.91, w). Due to the axial position of H-2, we can conclude that the Boc group might be oriented on the opposite site with respect to the carbonyl function at C-2.

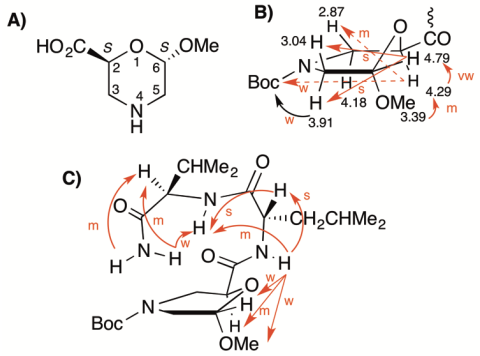

Figure 2. NOEs for peptide **7a**. A) Stereochemistry of morpholino ring. B) NOEs of morpholino ring protons. C) NOEs between the different amino acids.

NOEs between the proton backbone are shown in Figure 2C. Weak NOEs between NH_{Leu} and both OMe and H-6 were detected (Figure S3, ESI) indicating that NH_{Leu} is well oriented toward the oxygen region of the ring. A complete set of CH/NH (*i*, *i*+1), as well as NH/NH (*i*, *i*+1), NOEs is present (Figure S3, ESI).

Variable temperature NMR experiments (273-323 K), showing solvent protection due to the NH involvement in a H-bond,[33–35] were performed (Figure 3). Low variation of Δδ/ΔT values for all NHs (NH_{Leu} -1.8; NH_{Val} -1.9; NH_2 -2.7, -3.3 ppb) were detected. Considering these data and

according to the NOEs, our hypothesis is that NH_{Val} can be involved in a H-bond with CO_{Morph} forming a γ-turn. The very low Δδ/ΔT value for NH_{Leu}, together with its NOEs with the morpholino ring, supports the hypothesis of its H-bond with the oxygen of morpholino ring. Finally, a less stable H-bond was detected for NH_2 probably involving CO_{Morph} or CO_{Leu}.

Compound **7b**, differing from **7a** for the substituent at *C*-terminus, showed similar NOEs for the ring and backbone chain, although with different intensities (Figures S4-S6, ESI). Higher Δδ/ΔT value (Figure 3) was detected for NH_{Val} (-3.3 ppb/K), meaning that the γ-turn is less stable. The major stability of the γ-turn in peptide **7a** might be due to the $CONH_2$ contribution that reinforces the H-bond network. On the other hand, NH_{Leu} possesses a similar value indicating a similar behaviour as in **7a**.

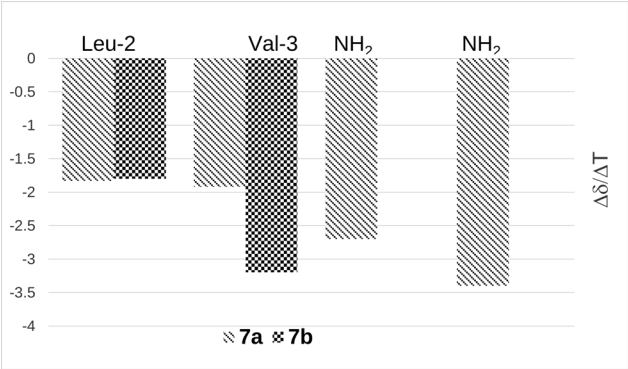

Figure 3. Δδ/ΔT NH values for peptides **7a** and **7b** (273-333 K).

A mixture of two isomers (60:40 ratio) was detected for pentapeptide **10**, as shown in NMR spectra. The morpholino ring is present in two different conformations (Figures S7A-S7B, ESI). The proton ring resonances and the $J_{H\text{-}2/H\text{-}3}$ values (*J* 11.0, 3.3 Hz) of the major isomer are similar to those of tripeptides **7**. The minor isomer **10'** differs both in the chemical shifts of the ring and, mostly, in the *J* values of H-2 (*J* 10.6, 6.4 Hz). NOEs similarities were detected for the protons of morpholino ring in the major (Figure S7A, ESI) and minor isomers (Figure S7B, ESI). Furthermore, the protons of an isomer show spatial proximities with the corresponding protons of the second one, indicating an equilibrium between the two isomers.[36]

Backbone chain NOEs are reported in Figure 4 (see also Figures S8-S11, ESI) only for the major isomer **10**.*

* Due to the overlapped signals or similar NOEs for the backbone protons of the two isomers, we were not able to identify the difference between the two conformers **10** and **10'**. Our hypothesis is that a γ-turn is present in both isomers at *C*-terminus.

As shown, analogous NOEs to **7a**, except for the intensity, were observed in the *C*-terminus region. The absence of spatial proximity between NH_2 and the morpholino ring or with the *N*-terminus dipeptide chain, excludes the formation of a β-turn.

The experiment at variable temperature (273-333 K, Δδ/ΔT: NH_{Val5} -2; NH_2 2.5 ppb; Figure 5) also showed similarities with **7a**, being Δδ/ΔT of NH_{Leu} the lowest one (-1.5 ppb). As a result, the γ-turn is confirmed in this case also, independently from the elongation of *N*-terminus chain.

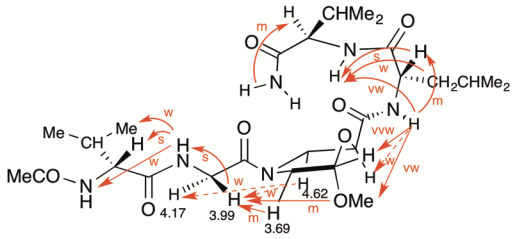

Figure 4. NOEs for peptide **10**.

Focusing on the *N*-terminus region, glycine possesses two diastereotopic protons in the main isomer (δ 3.99, 4.17) that, in general, are diagnostic for structured sequences.[37] The proton at higher field showed spatial proximity with H-3 (w), H-5 (m) and OMe (m) and that at lower filed with H-3 (w), suggesting the orientation of the chain on the opposite site with respect to the CO_{Morph}. Both CH/NH (i, i+1) and NH/NH (i, i+1) NOEs were shown. A low Δδ/ΔT (-2.2 ppb) was detected for NH_{Gly}. Taken together these data suggests the formation of a H-bond between this proton and $C{=}O_{Ac}$ (seven-member ring) with formation of a second γ-turn.

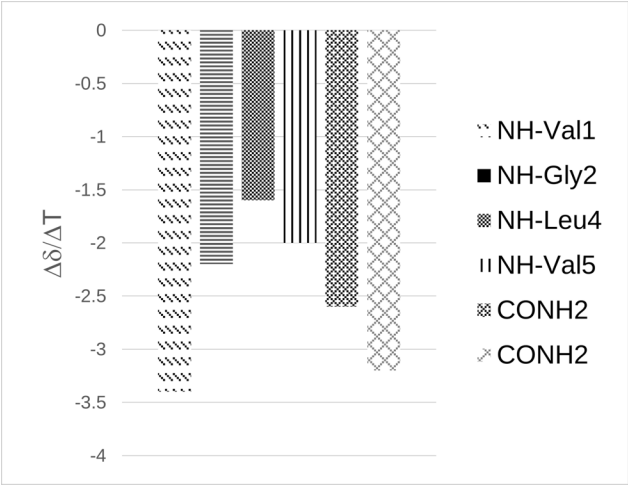

Figure 5. Δδ/ΔT NH values for peptide **10** (273-333 K).

Hexapeptide **12** is also present as a mixture of two isomers (**12/12'**: 60:40; NMR analysis). The proton signals were completely assigned for each isomer, except for Me groups and morpholine-1 that are overlapped. An equilibrium between the two isomers is documented by NOESY experiment

(see Figures S13-S16, ESI), as observed for **10**. The γ-turn is present both at *C*- and *N*-termini of β-Morf-Leu-Val motives. As shown in Figure 6, similar NOEs are present for NH_{Leu2} and NH_{Leu5} with the acetal region of the corresponding morpholine ring at position one and four. The main difference between the two conformers is the spatial proximity between the protons of β-Morf-4 and CH_{Val3}. In fact, this last proton shows proximity with H-3 in isomer **12** and with H-5 in isomer **12'** (Figure S13, ESI). These NOEs are diagnostic for the formation of *E*-isomer **12** and *Z*-isomer **12'** at the tertiary amide bond involving CO_{Val3} and the nitrogen of β-Morf-4.

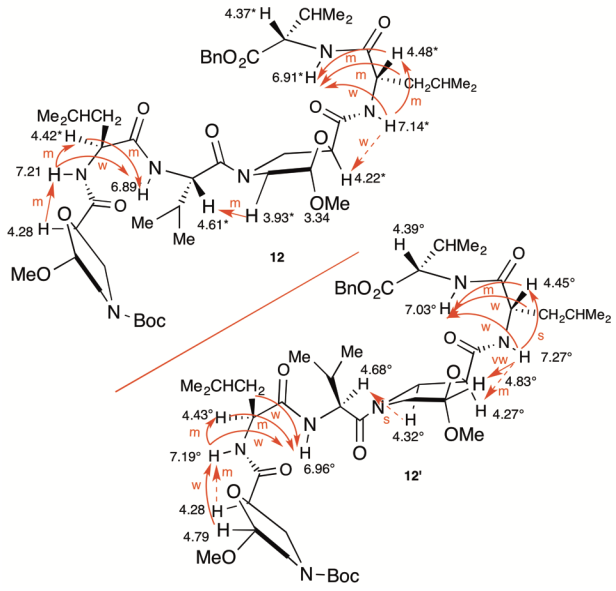

Figure 6. NOEs for isomers **12** and **12'**

Low variation of Δδ/ΔT values (273-323 K) for all NHs (Figure 7) was found for isomer **12**, showing a strong H-bond network. Based on the NOEs and Δδ/ΔT values, our hypothesis is that two γ–turns can be formed in hexapeptide **12**. Higher values were detected for *Z*-**12'**. Focusing on ppb/K values of valines, a lower propensity to give the γ-turn is evident for *Z*-1**2'** with respect to *E*-**12**. (Figure 7)

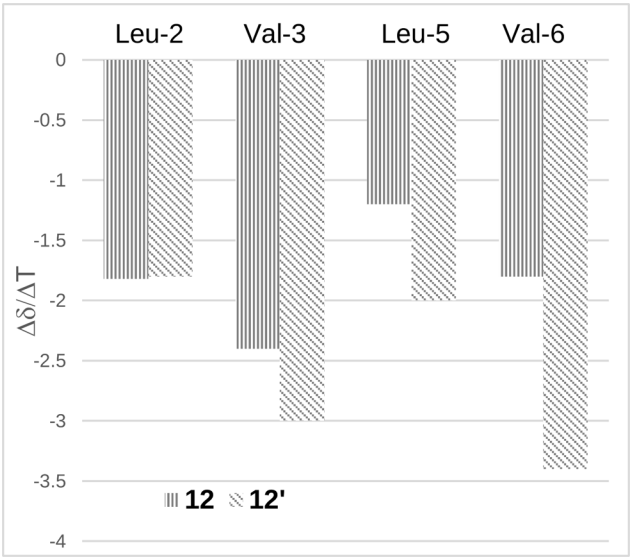

Figure 7. Δδ/ΔT NH values for peptide **12** (273-333 K).

To gain more information about the conformation of peptide **12,** far-UV circular dichroism (CD) analysis in CH_3CN (100 μM) was performed (Figure S25 in Supporting Information). Surprisingly, a negative minimum around 205 nm and a positive maximum around 230 nm indicate the polyproline II like profile.

IR studies of peptides. FTIR analysis was focused on the N-H stretching (amide A) region (~ 3500 cm^{-1}). Absorptions in this region are highly dependent on H-bond formation. Consequently, they are conformationally informative. In particular, it is known that, in the case of intramolecular hydrogen bonded conformations, the amide band A is downshifted in comparison with free NH group.[38] As shown in Figures 8 and S26 for peptides **7a,b** and **12**, the band at 3300 cm^{-1} is effectively more intense that the band at 3400 cm^{-1} in all peptides. This confirms the results of the NMR experiment at variable temperature, indicating the involvement of NH in H-bond.

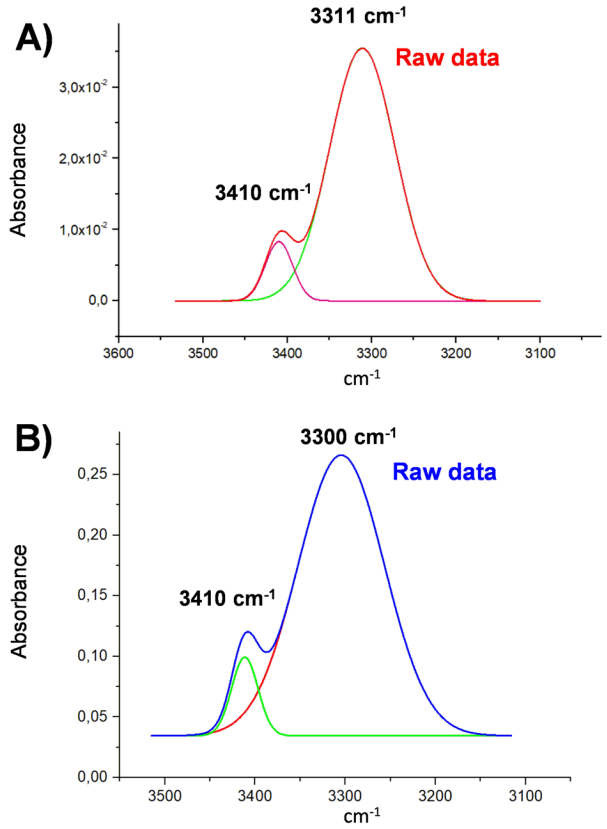

Figure 8. FTIR spectra of amide A portion acquired for peptide **7b** (A) and **12** (B).

Computational analysis of Peptides **7a** *and* **12**. Aiming to get additional insights into the folding attitude of (+)-β-Morph containing peptides, we performed computational analyses on peptides **7a** and **12**. In previous works, we used temperature replica exchange molecular dynamics (T-REMD)[39] to model linear and cyclic peptides containing non-coded amino acids.[17,18,33,36,40–45] In this work, we simulated peptides in acetonitrile solution to obtain a computational model as close as possible to experimental NMR conditions. Although T-REMD simulations can be performed with explicit solvation, they have a computational cost which can be prohibitive, since the number of required replicas is proportional to the number of particles in the system.[46] Thus, we selected accelerated molecular dynamics (aMD), a recent method that enhances the conformational sampling of complex molecules, such as biopolymers, at a reasonable computational cost,[47] especially when graphics processor units (GPU) are used.[48–50]

Tripeptide **7a** was subjected to a 1 μs aMD, a simulation time longer than that used for folding studies on larger peptides.[47] Cluster analysis performed on the last 250 ns of the aMD trajectory shows that two almost equivalent clusters (hereafter referred as cluster1 and cluster2, respectively) account for more than 70% of the whole conformational population. This suggests that two alternative conformations are possible for **7a**. The most representative conformations of cluster1

and 2 are depicted in Figure 9A and 9B, respectively, where representative geometrical parameters are also shown.

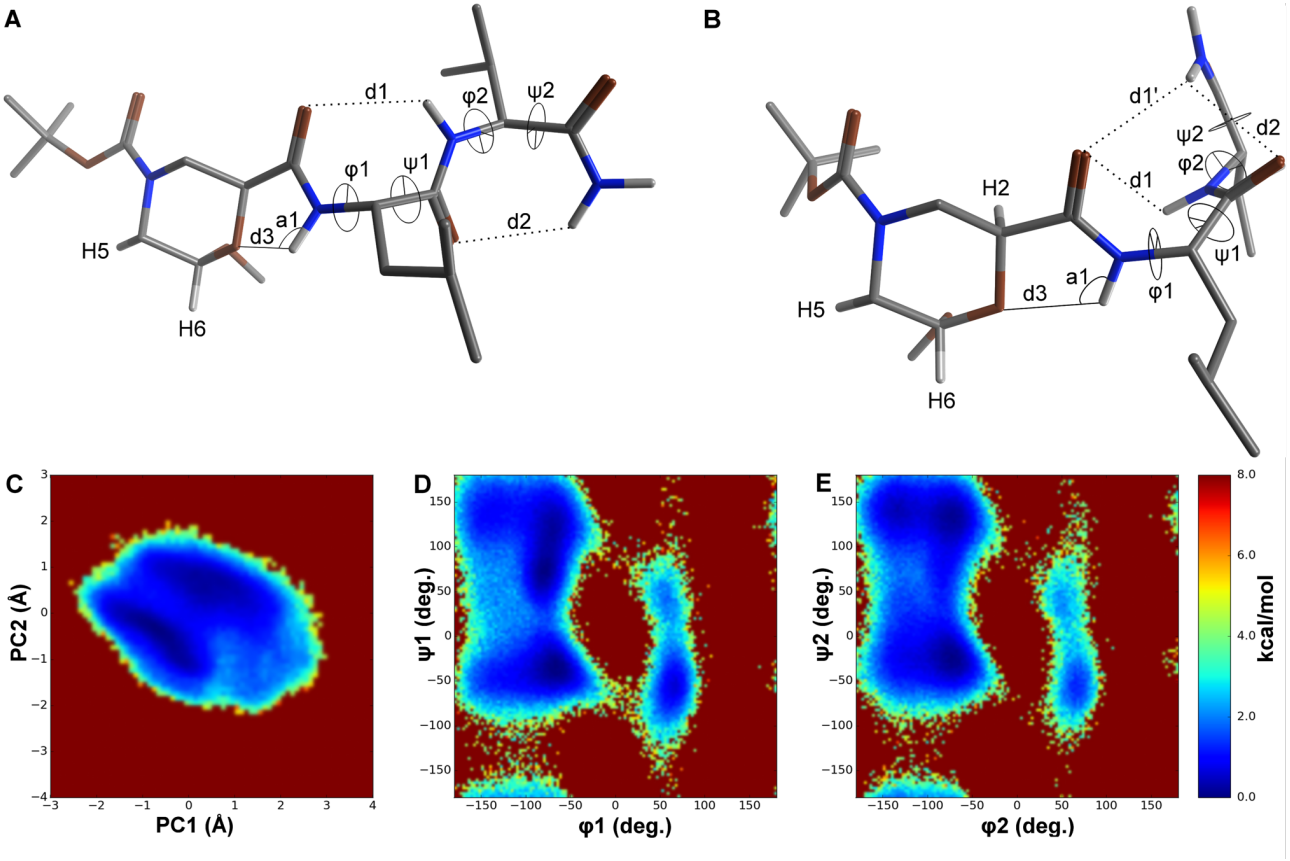

Figure 9. Most representative conformation of cluster1 [A), pop. = 35.5%] and cluster2 [B), pop. = 35.3%)] obtained from the analysis of the 750-1000 ns segment of the aMD trajectory of compound **7a**, conducted in explicit MeCN using the ff14SB force field. Distances are reported in Å, angles and dihedrals in deg. The values are taken from the non-minimized most representative conformation, while intervals are the mean deviations of the whole cluster population from the centroid. Selected geometrical parameters of cluster1 are: d1 = 2.7 ± 0.9; d2 = 2.6 ± 1.3; d3 = 2.2 ± 0.3; a1 = 109.9 ± 11.5; φ1 = -68.1 ± 25.3; ψ1 = 92.4 ± 31.0; φ2 = -72.3 ± 26.2; ψ2 = 77.5 ± 69.2. Selected geometrical parameters of cluster2 are: d1 = 3.6 ± 0.6; d1' = 3.2 ± 1.9; d2 = 2.6 ± 1.3; d3 = 2.1 ± 0.5; a1 = 112.3 ± 16.7; φ1 = -77.4 ± 19.5; ψ1 = -33.5 ± 16.3; φ2 = -94.0 ± 24.4; ψ2 = 40.1 ± 69.5. C) Reweighted free energy plot obtained from the projection of the first and second principal components (PC1 and PC2) of the 1 μs trajectory of **7a**. D) and E) Reweighted free energy plots of φ1 vs ψ1 and φ2 vs ψ2, respectively.

This was also confirmed by a principal component analysis (PCA), performed on the full trajectory, followed by projection of the Boltzmann reweighted[51] distribution onto the subspace defined by the first (PC1) and the second (PC2) principal component vectors describing 36% and 21% of the total motion, respectively (Figure 9C). The two dark blue regions centred at about -1.0, 0.5 and 0.2, 0.5 correspond to the two most relevant and similarly abundant conformations of compound **7a**.

The presence of two main conformational ensembles can also be observed by examining the Boltzmann reweighted distribution of relevant backbone dihedrals, depicted as free energy surfaces in Figure 9D and 9E. Analysing the φ1 vs ψ1 surface (Figure 9D), a rather deep well can be observed on the top left quarter, spanning from the polyproline helix to the γ-turn region. A second well, separated from the former by a relatively low energy saddle point, represents the α-helix region. The free energy surface of the second set of dihedrals (Figure 9E) shows that the terminal valine residue has a larger conformational freedom, and regions corresponding to the β-turn, the polyproline helix and the α-helix are frequently sampled. However, a low energy region corresponding to the γ-turn can still be noted. This suggests a fast equilibrium between PPI-like and a α-like conformation, mediated by a γ-turn.

This behaviour can be also appreciated by analysing the results from the cluster analysis. The representative geometry of cluster1 (Figure 9A), slightly more populated, presents a nice inverse γ-turn pattern, confirmed by d1 and d2 distances and by φ1, ψ1, φ2 and ψ2 dihedrals. This confirms that β-Morph have the quite rare ability to stabilise γ-turns.[7] Conversely, the most representative geometry of cluster2 (Figure 9B) is closer to a type I β-turn, as suggested by distance d1', indicating the possibility of an H-bond between the β-Morph carbonyl and the terminal NH_2 group, φ1/ψ1 and φ2/ψ2. NOE contacts detected by NMR (Figure 2) match most of the distances measured in both cluster 1 and 2 (Table 2). Additionally, φ1 and φ2 values in cluster1 and in cluster2 are compatible with a $J_{NH\text{-}CH\alpha}$ of about 8.5 Hz.[52]

Consistency between NOE signals and corresponding distances in cluster1 and cluster2 were analysed (Table 2). Apart some exceptions, the calculated distances fit very well with the experimental data, suggesting that the geometries of the two clusters are consistent with the experimental finding.

Table 2. Consistency between NOE signals and corresponding distances[a] in cluster1 and cluster2.[b]

NOE (strength)	**Cluster1**	**Cluster2**
β-MorphH5*cis* -H6 (s)	✓ (2.4 ± 0.1)	✓ (2.3 ± 0.2)
β-MorphH5*trans* -H6 (s)	✓ (2.5 ± 0.2)	✓ (2.6 ± 0.2)
β-MorphH2-H3*trans* (m)	✓ (3.1 ± 0.1)	✓ (3.0 ± 0.1)
β-MorphOMe-H2 (m)[c]	✓ (3.3 ± 0.6)	**?** (4.3 ± 0.6)
β-MorphOMe-NH_{Leu} (w)[c]	**?** (4.6 ± 0.8)	**?** (5.2 ± 0.6)
β-MorphH6-NH_{Leu} (w)	✓ (3.8 ± 0.4)	✓ (3.7 ± 0.6)
β-MorphH2-NH_{Leu} (m)	✓ (3.4 ± 0.4)	✓ (3.0 ± 0.4)

BOC-β-MorphH6 (w)[d]	✓ (3.9 ± 0.6)	✓ (3.6 ± 0.8)
BOC-β-MorphH2 (w)[d]	✗ (6.1 ± 0.6)	✓ (4.0 ± 2.1)
NH_{Leu}-$H\alpha_{Leu}$ (s)	✓ (2.8 ± 0.1)	✓ (2.8 ± 0.2)
$H\alpha_{Leu}$-NH_{Val} (s)	✓ (2.2 ± 0.2)	**?** (3.5 ± 0.1)
NH_{Leu}-NH_{Val} (m)	**?** (4.2 ± 0.3)	✓ (2.9 ± 0.4)
$H\alpha_{Val}$-NH_2*trans* (m)	✓ (2.5 ± 0.5)	✓ (3.1 ± 0.6)
ValHα-NH_2*cis* (m)	✓ (3.4 ± 0.3)	**?** (3.8 ± 0.2)
NH_{Val}-NH_2*trans* (w)	✓ (4.0 ± 0.8)	✓ (3.0 ± 0.9)

[a]All distances, in Å are taken from the non-minimized most representative conformation of each cluster, while intervals are the mean deviations from the cluster centroid. [b]✓ computed distance is compatible with NOE signal. ✗ computed distance is larger than expected for matching NOE signal. **?** computed distance is larger than expected, but might be compatible with NOE signal. NOE signals are classified as strong (s), medium (m) and weak (w). [c]Distance measured from OMe carbon atom. [d]Distance measured from the BOC methyl carbon, averaged among the three methyl groups.

Most of the contacts within the morpholine ring are satisfied in both geometries. The β-MorphH6-NH_{Leu} distance matches with the observed NOE signal (Figure 2) in both clusters, confirming the peculiar stability of the pseudo 5-membered ring formed by β-Morph O, Cα and C=O, and by NH_{Leu}. Indeed, distance d3 (Figures 9A,B) suggests an H-bond between NH_{Leu} and the β-Morph ring oxygen, also suggested by the Δδ/δT value (Figure 3), even if the N-H···O angle (109.9 ± 11.5 deg.) is below the threshold for classical H-bonds.[53] To understand if this interaction can be considered as a true H-bond, we performed a quantum theory of atoms in molecules (QTAIM) analysis on the most representative geometry of cluster1, previously optimized in the gas phase by density functional theory (DFT) using the mPW1B95/6-31+G(d,p) level of theory, as done in previous works.[41,43,54] Interestingly, we observed a bond critical point (BCP) and a bond path connecting NH_{Leu} to β-Morph oxygen (Figure S17, ESI). The BCP density $\rho(r_c)$ = 0.021 a.u. is within the range of classical H-bonds (0.002-0.022 a.u.)[55,56] and is comparable to those obtained for the $C{=}O_{Leu}\cdots HN_{Val}$ and $C{=}O_{Val}\cdots H_2N$ (0.021 and 0.022 a.u., respectively) H-bonds observed in the same geometry. Thus, we can conclude that the H-bond between NH_{Leu} and the morpholine oxygen might be important in determining the conformational preferences of β-Morph containing peptides.

Concerning the hexapeptide **12**, NMR experiments shown the presence of two isomers (**12** and **12'**, Figure 6), probably due to the *E/Z* isomerism around the tertiary amide bond between Val3 and β-Morph4. In the adopted conditions, aMD simulations were not able to sample any event of ω isomerization due to the relatively high energy barrier for the process, estimated around 17 kcal/mol

for related compounds.[44] Thus, aMD simulations were conducted in the same conditions on both *E*-**12** and *Z*-**12'**. The cluster analysis of *E*-**12** showed two principal conformational clusters, accounting for more than 80% of the total population and having a clear prevalence for cluster1 over cluster2 (population = 44.3% and 29.2%, respectively). The most representative geometry of cluster1 (Figure 10) is well-structured: two i→i+2 H-bonds, typical of γ-turns, are found between the carbonyl groups of β-Morph1 and 4 and NH_{Val3} and NH_{Val6}, respectively.

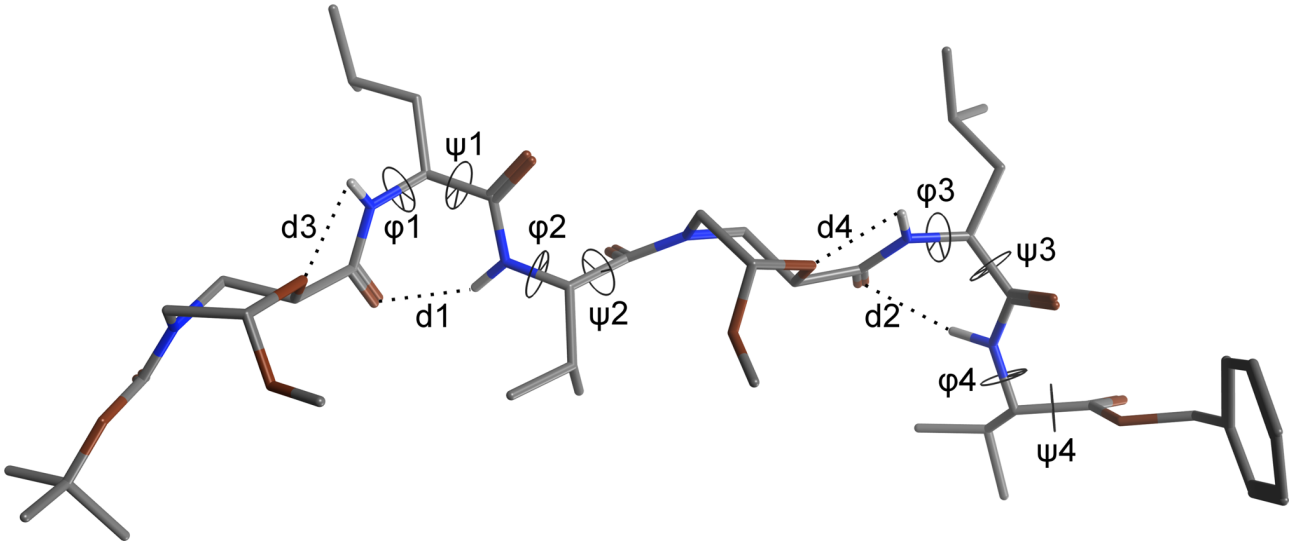

Figure 10. Most representative conformation of cluster1 (pop. = 44.3%) obtained from the analysis of the 750-1000 ns segment of the aMD trajectory of hexapeptide *E*-**12**, conducted in explicit CH_3CN using the ff14SB force field. Selected geometrical parameters are: d1 = 2.1 ± 1.4; d2 = 2.2 ± 1.4; d3 = 2.4 ± 0.3; d4 = 2.2 ± 0.4; φ1 = -77.5 ± 24.7; ψ1 = 60.9 ± 56.7; φ2 = -61.2 ± 34.8; ψ2 = 134.9 ± 19.6; φ3 = -82.6 ± 28.5; ψ3 = 80.8 ± 65.4; φ4 = -42.3 ± 52.9; ψ4 = 97.2 ± 60.3. Distances are reported in Å, dihedrals in deg. The values are taken from the non-minimized most representative conformation, while intervals are the mean deviations of the whole cluster population from the centroid.

Cluster2 (Figure S18, ESI) has geometrical parameters similar to cluster1 (Figure 10), except for the ψ1 dihedral. This falls in the helix region of the Ramachandran plot (ψ1 = -51.6 ± 25.6) and breaks the inverse γ-turn between β-Morph1 and Val3 observed in cluster1. On the other hand, the second γ-turn, involving β-Morph4 and Val6, remains intact. Indeed, in both clusters, φ1 and φ3 are constrained to a value of about -70 deg., as also observed for **7a**, confirming the peculiar behaviour of the β-Morph scaffold in determining the conformation of these peptides.

The analysis of the free energy surfaces obtained from the Boltzmann reweighted distribution of all four φ and ψ pairs (Figure S19, ESI) confirms the possibility of φ1 and φ3 to principally sample a region around -75 deg., while ψ1 and ψ3 can adopt values typical of the polyproline region (about

150 deg.), the inverse γ-turn (about 70 deg.) and the α-helix (about -50 deg.). Conversely, the φ2/ψ2 and φ4/ψ4 pairs, belonging to the two Leu-Val segments, adopt conformations typical of the extended/polyproline region, with the latter dihedral pair being less conformationally constrained due to its terminal nature. Both cluster1 and 2 geometries fit well with NOE data (Table S7, ESI), matching most of the distances detected for compound *E*-**12,** thus confirming the possibility of a conformational equilibrium between the two structures.

In the case of *Z*-**12'**, a principal cluster (cluster1, pop. = 38.3%; Figure 11) and two secondary clusters (cluster2, pop. = 16.9%, cluster3, pop. = 14.6%); Figure S20, ESI) were observed. Surprisingly, cluster1 geometry is represented by a helix-like structure, not observed from *E*-**12** simulations. Such geometry is stabilized by two i→i+4 H-bonds between $C{=}O_{\beta\text{-Morph1}}$ and NH_{Leu5} and between $C{=}O_{Leu2}$ and NH_{Val6}, having lengths (d1 and d2; Figure 11) and N-H···O angles (166.9 ± 59.8 and 169.9 ± 23.6 deg.) close to ideal for H-bonding. The φ1 dihedral is comparable to that observed for the main cluster of *E*-**12**, while φ3 is a little narrower but sill of the same sign. Conversely, ψ1 and ψ3 dihedrals prevalently assume negative values, typical of helical secondary structures. This behaviour is confirmed by the free energy distributions of φ1/ψ1 and φ3/ψ3 dihedral pairs (Figures S21A,C, ESI), showing a rather deep energy well in the helix region, while the energy minima corresponding to the polyproline and γ-turn regions seems to be less favourable, compared to *E*-**12** (Figures S19A,C, ESI). Not much difference between the two isomers is instead observed when comparing the free energy distributions of φ2/ψ2 and φ4/ψ4 pairs, belonging to the Leu-Val portions (Figures S19B,D and S21B,D, ESI).

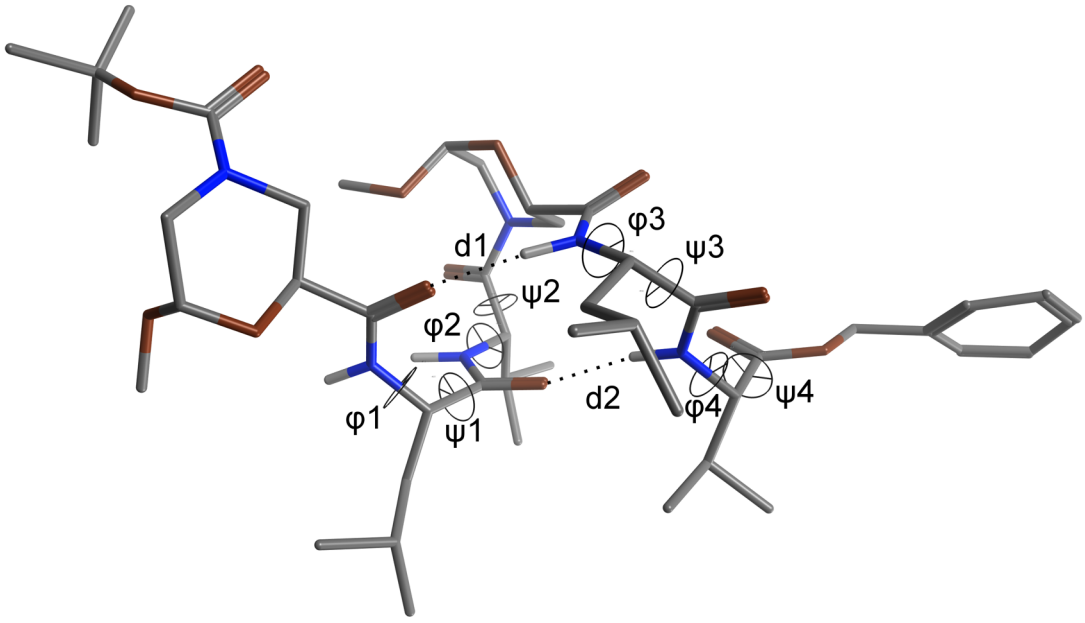

Figure 11. Most representative conformation of cluster1 (pop. = 38.3%) obtained from the analysis of the 750-1000 ns segment of the aMD trajectory of hexapeptide *Z*-**12'**. Selected geometrical parameters are: d1 = 1.9 ± 0.4; d2 = 2.1 ± 1.1; φ1 = -86.1 ± 16.5; ψ1 = -42.7 ± 39.0; φ2 = -135.4 ± 46.2; ψ2 = 94.7 ± 14.2; φ3 = -50.1 ± 20.8; ψ3 = -43.3 ± 23.1; φ4 = -91.7 ± 22.2; ψ4 = 128.5 ± 41.2. Distances are reported in Å, dihedrals in deg. The values are taken from the non-minimized most representative conformation, while intervals are the mean deviations of the whole cluster population from the centroid.

On the other hand, cluster2 (Figure S20A, ESI), is characterized by backbone dihedrals of the same sign as those observed for *E*-**12**. However, the H-bonds typical for the γ-turn, observed in both **7a** and *E*-**12**, are not detected in this geometry (see d1 and d2 distances, Figure S20A). Moreover, ψ1 and ψ3 dihedrals (128.5 ± 29.6 and 139.2 ± 54.9 deg., respectively) are wider, compared to *E*-**12**, and fall in the polyproline region. Cluster3 (Figure S20B) has selected distances and dihedrals comparable to those of cluster2 but assumes a U-like shape. This can be due to the inverted chair conformation of β-Morph4, probably stabilized by the dispersive interactions between the *N*-terminal BOC and the *C*-terminal benzyl group. Interestingly, cluster1-3 geometries match rather well the NOE signals detected for *Z*-**12'** (Table S8, ESI), confirming that a conformational equilibrium between these three structures might be possible. To assess if the conformational behaviour of the hexapeptide could also be influenced by the *E*/*Z* isomerization of the BOC group linked to β-Morph1, the aMD simulation was repeated for the *Z*-BOC-β-Morph1/*Z*-Val3-β-Morph4 isomer (*Z*1,*Z*4-**12'**). However, results were comparable to those obtained for *Z*-**12'** (Figure S22, ESI).

Although the above aMD simulations provided data consistent with NMR experiments, some doubts still needed to be solved. First, we observed that aMD, at least in the adopted conditions, was not able to sample ω rotation. Consequently, it is not possible, based on the above data, to make any consideration on the relative population of the *E*- or *Z*-isomers. Moreover, free energy surfaces from aMD dihedral distributions need reweighting to recover the original (unbiased) torsional potential. Different reweighting protocols are reported by literature,[51,57] and choosing the proper method is not trivial.[58] For these reasons, we deserved to confirm our results by using a different method. Hamiltonian replica exchange molecular dynamics (H-REMD) is an enhanced sampling method where the system Hamiltonian (*i.e.* the force field), instead of temperature, is the exchanging coordinate.[46,59] Since only a limited subset of the system degrees of freedom is affected by Hamiltonian exchange, H-REMD simulations need a lower number of replicas than T-REMD, thus making H-REMD a powerful method to study biomolecular folding in explicit solvent.[60]

In this work, we performed H-REMD simulations on compound **12**, by progressively lowering the torsional potential of all the φ, ψ and ω dihedrals over 12 replicas (see methods in ESI). Two separate runs were conducted by starting from *E*-**12** and from *Z*1,*Z*4-**12'**. The simulation length was determined based on full convergence between the two runs, in terms of distributions of ω dihedrals, free energy surface of φ/ψ distributions, cluster populations and RMSD between the coordinates of representative conformations of principal clusters. A complete convergence between the two runs was obtained after about 1.5 μs, so simulations were carried out for 2.0 μs. All the analyses were then performed on the 1.5 – 2.0 μs sector of the unbiased replica.

As expected, the free energy distributions of relevant φ/ψ pairs (Figure S23, ESI) look like a combination of those obtained by aMD for *E*-**12** and *Z*-**12'** configurations (Figures S19 and S21, ESI). Moreover, clustering analysis resulted in three main clusters having a population above 15%. Cluster1 (pop. = 22.8%, Figure S24A, ESI) has an *E* configuration at ω4 and is comparable to the geometry of cluster1 obtained from the aMD simulation on *E*-**12**, except for the ω1 dihedral (between BOC and β-Morph) which is *Z*. Cluster2 (Pop. = 20.2%) has a *Z*-ω4 configuration and adopts a helix-like conformation comparable to that observed for cluster1 from the aMD simulations of *Z*-**12'**. Cluster3 (pop. = 15.7%) has an all-*E* configuration of ω dihedrals and is comparable to the cluster2 geometry obtained from the aMD simulations of *E*-**12**. These results confirm aMD as a powerful tool for analysing the conformational preference of non-natural peptides, providing results comparable to those produced by much more CPU-intensive simulations (about 150 ns/day on 288 Xeon E5-2600 v4 cores vs 230 ns/day on one GTX Titan Black GPU card for H-REMD and aMD, respectively). However, some attention should be paid when the rotation of amide bonds is critical, as might occur in peptides containing proline or non-proteogenic proline analogues.

Conclusion

The new cyclic enantiopure β-Morph (**1**) was prepared in gram scale from the inexpensive and enantiopure D-glucopyranose. NMR data and computational simulations show that β-Morph can induce an inverse γ-turn when precedes the dipeptide sequence Leu/Val, that typically prefers an extended conformation. These experiments suggest the presence of an H-bond between the oxygen of the morpholino ring and the NH of the amino acid at position i+1. This H-bond might favour the γ-turn by providing an additional constraint that forces the first φ dihedral after β-Morph (φ1 and φ3 in **7a** and **12**) to adopt values around -75 deg., typical of the γ-turn. Furthermore, even if cyclic β-

amino acids are able to induce turn conformations to be used for building hairpins,[22] this H-bond probably prevents the formation of this motif, as demonstrated for longer peptides **10** and **12**.

The repeating β-Morph/Leu/Val motif in peptide **12** can lead to the formation of two γ-turns. However, MD simulations show that an equilibrium between additional geometries might be possible due to the ability of ψ1 and ψ3 dihedral to span between the polyproline and the α-helix region. The polyproline II like architecture is also confirmed by far-UV circular dichroism (CD). This conformational propensity might be affected by the *E/Z* isomerism at the amide bond involving β-Morph nitrogen. Nevertheless, we expect that an additional control over the conformational preferences of β-Morph containing peptides might be obtained by exploring different substituents at the morpholino ring.

Acknowledgements

AC is grateful to CINECA for providing access to HPC infrastructure.

E-mail: marialuisa.gelmi@unimi.it

† Electronic supplementary information (ESI) available: Description of synthetic procedures and characterization of compounds. NMR additional data. Computational methods and additional Figures and Tables.

References

1 E. J. Milner-White, B. M. Ross, R. Ismail, K. Belhadj-Mostefa and R. Poet, *J. Mol. Biol.*, 1988, **204**, 777–782.

2 K. Guruprasad and S. Rajkumar, *J. Biosci.*, 2000, **25**, 143–156.

3 B. W. Matthews, *Macromolecules*, 1972, **5**, 818–819.

4 B. Walse, J. Kihlberg and T. Drakenberg, *Eur. J. Biochem.*, 1998, **252**, 428–440.

5 L. Kirnarsky, O. Prakash, S. M. Vogen, M. Nomoto, M. A. Hollingsworth and S. Sherman, *Biochemistry*, 2000, **39**, 12076–12082.

6 H. E. Bleich, R. E. Galardy and M. P. Printz, *J. Am. Chem. Soc.*, 1973, **40**, 2041–2042.

7 M. Crisma, M. De Zotti, A. Moretto, C. Peggion, B. Drouillat, K. Wright, F. Couty, C. Toniolo and F. Formaggio, *New J. Chem.*, 2015, **39**, 3208–3216.

8 D. Mazzier, L. Grassi, A. Moretto, C. Alemán, F. Formaggio, C. Toniolo and M. Crisma, *J. Pept. Sci.*, 2017, **23**, 346–362.

9 F. Sladojevich, A. Guarna and A. Trabocchi, *Org. Biomol. Chem.*, 2010, **8**, 916–924.

10 J. L. Baeza, G. Gerona-Navarro, M. J. P. de Vega, M. T. García-López, R. González-Muñiz and M. Martín-Martínez, *Tetrahedron Lett.*, 2007, **48**, 3689–3693.

11 D. Yang, W. Li, J. Qu, S. W. Luo and Y. D. Wu, *J. Am. Chem. Soc.*, 2003, **125**, 13018–13019.

12 A. Bonetti, F. Clerici, F. Foschi, D. Nava, S. Pellegrino, M. Penso, R. Soave and M. L. Gelmi, *European J. Org. Chem.*, 2014, **15**, 3203–3209.

13 M. Penso, F. Foschi, S. Pellegrino, A. Testa and M. L. Gelmi, *J. Org. Chem.*, 2012, **77**, 3454–3461.

14 A. Ruffoni, A. Casoni, S. Pellegrino, M. L. Gelmi, R. Soave and F. Clerici, *Tetrahedron*, 2012, **68**, 1951–1962.

15 S. Pellegrino, F. Clerici and M. L. Gelmi, *Tetrahedron*, 2008, **64**, 5657–5665.

16 R. Bucci, S. Giofré, F. Clerici, A. Contini, A. Pinto, E. Erba, R. Soave, S. Pellegrino and M. L. Gelmi, *J. Org. Chem.*, 2018, **83**, 11493–11501.

17 S. Pellegrino, N. Tonali, E. Erba, J. Kaffy, M. Taverna, A. Contini, M. Taylor, D. Allsop, M. L. Gelmi and S. Ongeri, *Chem. Sci.*, 2017, **8**, 1295–1302.

18 A. Contini, N. Ferri, R. Bucci, M. G. Lupo, E. Erba, M. L. Gelmi and S. Pellegrino, *Biopolymers*, 2017, 1–8.

19 S. Pellegrino, G. Facchetti, A. Contini, M. L. Gelmi, E. Erba, R. Gandolfi and I. Rimoldi, *RSC Adv.*, 2016, **6**, 71529–71533.

20 S. Pellegrino, A. Bonetti, F. Clerici, A. Contini, A. Moretto, R. Soave and M. L. Gelmi, *J. Org. Chem.*, 2015, **80**, 5507–5516.

21 A. Bonetti, S. Pellegrino, P. Das, S. Yuran, R. Bucci, N. Ferri, F. Meneghetti, C. Castellano, M. Reches and M. L. Gelmi, *Org. Lett.*, 2015, **17**, 4468–4471.

22 B. R. Huck, J. D. Fisk and S. H. Gellman, *Org. Lett.*, 2000, **2**, 2607–2610.

23 N. Burdzhiev, E. Stanoeva, B. Shivachev and R. Nikolova, *Comptes Rendus Chim.*, 2014, **17**, 420–430.

24 F. Tratar, G. Marc, M. Sollner and D. Kikelj, *Arkivoc*, 2001, **(v)**, 7–20.

25 E. Sikorska, D. Tuwalska, P. Karpowicz, E. Jankowska, A. Nowacki and B. Liberek, *Tetrahedron*, 2015, **71**, 2013–2024.

26 A. Franconetti, S. Jatunov, P. Borrachero, M. Gómez-Guillén and F. Cabrera-Escribano, *Org. Biomol. Chem.*, 2013, **11**, 676–686.

27 J. F. Billing and U. J. Nilsson, *Tetrahedron*, 2005, **61**, 863–874.

28 R. Volkmer-Engert, B. Hoffmann and J. Schneider-Mergener, *Tetrahedron Lett.*, 1997, **38**, 1029–1032.

29 E. G. Von Roedern, E. Lohof, G. Hessler, M. Hoffmann and H. Kessler, *J. Am. Chem. Soc.*, 1996, **118**, 10156–10167.

30 A. Hagarman, T. J. Measey, D. Mathieu, H. Schwalbe and R. Schweitzer-Stenner, *J. Am. Chem. Soc.*, 2010, **132**, 540–551.

31 P. A. Burland, H. M. I. Osborn and A. Turkson, *Bioorg. Med. Chem.*, 2011, **19**, 5679–5692.

32 K. C. Nicolaou, Y. He, K. C. Fong, W. H. Yoon, H.-S. Choi, Y.-L. Zhong and P. S. Baran, *Org. Lett.*, 1999, **1**, 63–66.

33 A. Ruffoni, A. Contini, R. Soave, L. Lo Presti, I. Esposto, I. Maffucci, D. Nava, S. Pellegrino, M. L. Gelmi and F. Clerici, *RSC Adv.*, 2015, **5**, 32643–32656.

34 G. M. Bonora, C. Mapelli, C. Toniolo, R. R. Wilkening and E. S. Stevens, *Int. J. Biol. Macromol.*, 1984, **6**, 179–188.

35 J. D. Augspurger, V. A. Bindra, H. A. Scheraga and A. Kuki, *Biochemistry*, 1995, **34**, 2566–2576.

36 R. Bucci, A. Bonetti, F. Clerici, A. Contini, D. Nava, S. Pellegrino, D. Tessaro and M. L. Gelmi, *Chem. - A Eur. J.*, 2017, **23**, 10822–10831.

37 K. Tonan and S. Ikawa, *Spectrochim. Acta Part A Mol. Biomol. Spectrosc.*, 2003, **59**, 111–120.

38 A. Barth, *Biochim. Biophys. Acta - Bioenerg.*, 2007, **1767**, 1073–1101.

39 Y. Sugita and Y. Okamoto, *Chem. Phys. Lett.*, 1999, **314**, 141–151.

40 S. Pellegrino, A. Contini, F. Clerici, A. Gori, D. Nava and M. L. Gelmi, *Chem. – A Eur. J.*,

2012, **18**, 8705–8715.

41 I. Maffucci, S. Pellegrino, J. Clayden and A. Contini, *J. Phys. Chem. B*, 2015, **119**, 1350–1361.

42 M. Tomsett, I. Maffucci, B. A. F. Le Bailly, L. Byrne, S. M. Bijvoets, M. G. Lizio, J. Raftery, C. P. Butts, S. J. Webb, A. Contini and J. Clayden, *Chem. Sci.*, 2017, **8**, 3007–3018.

43 I. Maffucci, J. Clayden and A. Contini, *J. Phys. Chem. B*, 2015, **119**, 14003–13.

44 L. Ricci, L. Sernissi, D. Scarpi, F. Bianchini, A. Contini and E. G. Occhiato, *Org. Biomol. Chem.*, 2017, **15**, 6826–6836.

45 L. Sernissi, L. Ricci, D. Scarpi, F. Bianchini, D. Arosio, A. Contini and E. G. Occhiato, *Org. Biomol. Chem.*, 2018, **16**, 3402–3414.

46 N. Rathore, M. Chopra and J. J. de Pablo, *J. Chem. Phys.*, 2005, **122**, 024111.

47 L. C. T. Pierce, R. Salomon-Ferrer, C. Augusto F. de Oliveira, J. A. McCammon and R. C. Walker, *J. Chem. Theory Comput.*, 2012, **8**, 2997–3002.

48 S. Le Grand, A. W. Götz and R. C. Walker, *Comput. Phys. Commun.*, 2013, **184**, 374–380.

49 R. Salomon-Ferrer, A. W. Götz, D. Poole, S. Le Grand and R. C. Walker, *J. Chem. Theory Comput.*, 2013, **9**, 3878–3888.

50 A. W. Götz, M. J. Williamson, D. Xu, D. Poole, S. Le Grand and R. C. Walker, *J. Chem. Theory Comput.*, 2012, **8**, 1542–1555.

51 W. Sinko, Y. Miao, C. A. F. de Oliveira and J. A. McCammon, *J. Phys. Chem. B*, 2013, **117**, 12759–12768.

52 F. Li, J. H. Lee, A. Grishaev, J. Ying and A. Bax, *ChemPhysChem*, 2015, **16**, 572–578.

53 E. Arunan, G. R. Desiraju, R. A. Klein, J. Sadlej, S. Scheiner, I. Alkorta, D. C. Clary, R. H. Crabtree, J. J. Dannenberg, P. Hobza, H. G. Kjaergaard, A. C. Legon, B. Mennucci and D. J. Nesbitt, *Pure Appl. Chem.*, 2011, **83**, 1637–1641.

54 A. Contini and E. Erba, *RSC Adv.*, 2012, **2**, 10652.

55 U. Koch and P. L. A. Popelier, *J. Phys. Chem.*, 1995, **99**, 9747–9754.

56 T.-H. Tang, W.-J. Hu, D.-Y. Yan and Y.-P. Cui, *J. Mol. Struct. THEOCHEM*, 1990, **207**, 319–326.

57 Y. Miao, W. Sinko, L. Pierce, D. Bucher, R. C. Walker and J. A. McCammon, *J. Chem. Theory Comput.*, 2014, **10**, 2677–2689.

58 Z. Jing and H. Sun, *J. Chem. Theory Comput.*, 2015, **11**, 2395–2397.

59 S. Jang, S. Shin and Y. Pak, *Phys. Rev. Lett.*, 2003, **91**, 058305.

60 M. Meli, G. Colombo, M. Meli and G. Colombo, *Int. J. Mol. Sci.*, 2013, **14**, 12157–12169.